Training and Testing Machine Learning Algorithms for VSLLIM Reactor Controller

Mohamed S. El-Genk, Timothy M. Schriener, Ahmad N. Shaheen
Institute for Space and Nuclear Power Studies and Nuclear Engineering
Department, University of New Mexico, Albuquerque, NM, USA

Technical Work Scope: DOE Office of Nuclear Energy's Nuclear Energy University Programs contract DE-NE0009268 subaward from Purdue University to the University of New Mexico (UNM).

Performance Period: 01-01-2023 to 03-31-2024

Report No. UNM-ISNPS-01-2024
Institute for Space and Nuclear Power Studies, The University of New Mexico,
Albuquerque, NM, USA, http://isnps.unm.edu/reports/

April 2024

Training and Testing Machine Learning Algorithms for VSLLIM Reactor Controller

Mohamed S. El-Genk, Timothy M. Schriener, Ahmad N. Shaheen
Institute for Space and Nuclear Power Studies and Nuclear Engineering Department
The University of New Mexico, Albuquerque, NM

Abstract

The research team at the University of New Mexico's Institute for Space and Nuclear Power Studies (UNM-ISNPS) investigated training and evaluating the performance of an artificial Intelligence (AI) controller, based on an artificial neural network, for the **V**ery-**S**mall, **L**ong-**LI**fe, **M**odular (**VSLLIM**) microreactor design developed at UNM-ISNPS. The walk-away safe VSLLIM microreactor for generating between 1.0 – 10 MW_{th} is fully passive with redundant safety and operation features. Natural circulation of the in-vessel sodium coolant cools the core during nominal operation and for decay heat removal after shutdown with the aid of the in-vessel chimney and helical coiled tubes Na/Na heat exchanger. The integrated power system with a VSLLIM reactor with a Na-Air heat exchanger and open-air Brayton cycle transported together on an 18-wheeler truck to its destination. This system for energy generation in arid regions can generate 10.0 and 1.0 MW_{th} continuously 24/7 without refueling for 5.9 and 91 years, respectively.

1. Objectives

The objectives for this task at UNM-ISNPS are to: (a) develop a physics-based transient model of the VSLLIM reactor, which couples reactor kinetics and thermal-hydraulics, using the modular MATLAB Simulink platform [The MathWorks, 2022], (b) use the developed reactor model to generate training data for a transient startup scenario of the nuclear reactor from initial subcritical condition to nominal steady state operation, (c) develop a neural network Machine Learning (ML) algorithm and train it using the data generated using the developed transient model of simulated startup transients, and (d) perform parametric analyses to investigate the performance the ML algorithm and test the performance of the AI controller for real-time control of the reactor.

2. VSLLIM Microreactor

The walk-away safe VSLLIM microreactor design developed at UNM-ISNPS offers many passive operation and safety features and is cooled by natural circulation of in-vessel liquid sodium during nominal operation and for decay heat removal with the aid of in-vessel helically coiled tubes Na/Na heat exchanger and 2 m tall chimney [El-Genk and Palomino 2019; El-Genk, Schriener, and Palomino 2021]. The reactor can continuously generate 10 - 1.0 MW of thermal power for ~5.9 - 92 Full Power Years (FPY), respectively, without refueling. The VSLLIM is to be constructed, assembled, and sealed in the factory, before being integrated to the balance of the power generation system and transported to the operating site on an 18-wheeler truck (Fig. 1).

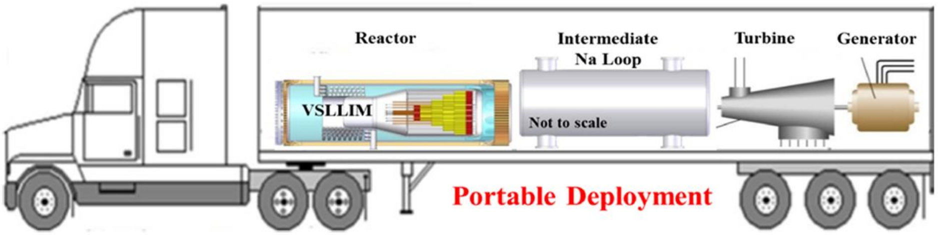

Fig. 1: VSLLIM microreactor plant mounted on an 18-wheelers truck.

The module VSLLIM microreactor can also be installed below ground, to protect against missile attack or an airplane crash, and mounted on seismic isolation bearings to protect against earthquakes (Fig. 2). The reactor can provide both electricity and process heat for space heating and industrial uses and is compatible with different energy conversion options for electricity generation, such as superheated steam Rankine cycle, supercritical CO_2 Brayton cycle, and open-air Brayton cycle in arid regions (Fig. 1).

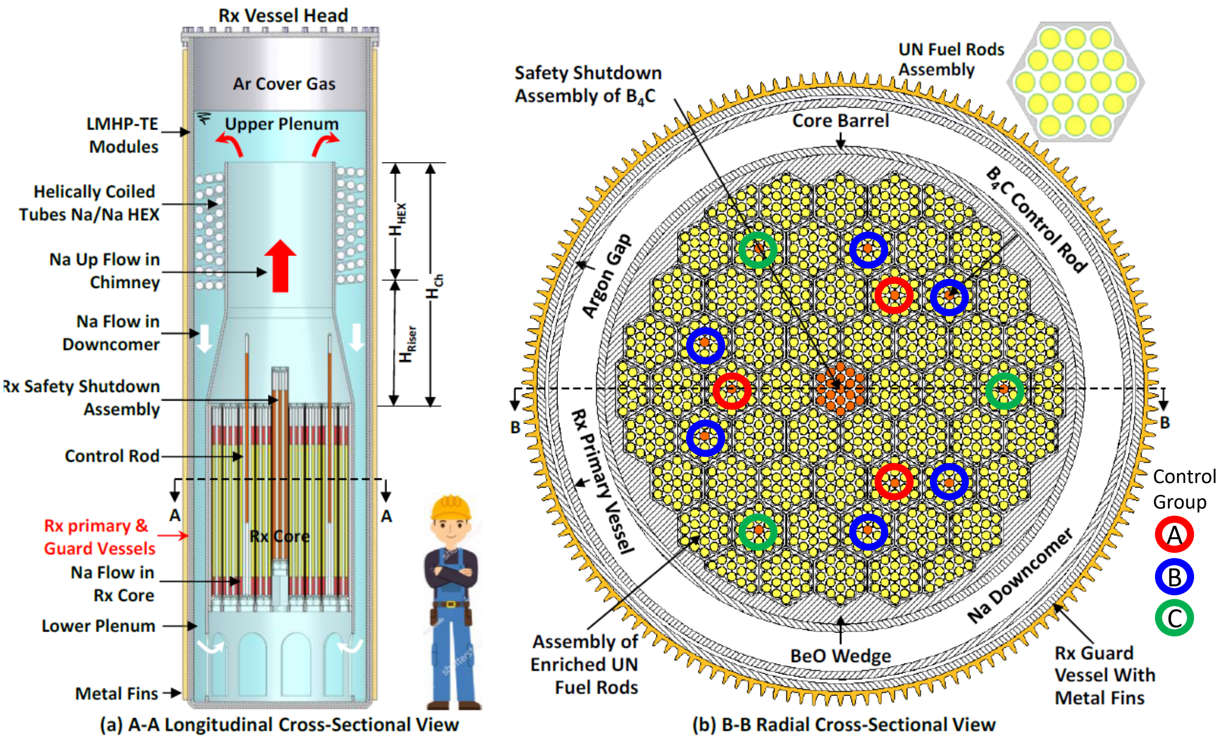

(a) A-A Longitudinal Cross-Sectional View

(b) B-B Radial Cross-Sectional View

Fig. 2: Longitudinal and radial cross section views of the VSLLIM microreactor for generating 1-10 MW_{th} showing sodium flow path and locations of reactor control rod groups.

Natural circulation of the in-vessel liquid sodium cools the nuclear reactor core during nominal operation and after shutdown (Figs. 2-3) [El-Genk and Palomino 2019], aided by a 2 m tall chimney, and in-vessel helically coiled tubes Na/Na heat exchanger (HEX) located at the top of the downcomer (Figs. 2-4). Owing to the low vapor pressure of sodium, the VSLLIM microreactor operates slightly below atmospheric pressure eliminating the need for a pressure vessel. Instead, the reactor has a primary vessel and a guard vessel, separated with a small gap filled with argon gas that houses sodium leak detectors. The argon gas decreases losses of thermal power for the reactor during operation to the environment. In the event of a loss of heat removal due to a failure or malfunction of the in-vessel Na/Na HEX, the argon gas is discharged and the gap between the primary and guard vessels is flooded with liquid sodium to facilitate the decay heat removal by in-vessel natural circulation. The removed decay is removed from the outer surface of reactor guard vessel using natural circulation of ambient air [Palomino, El-Genk, Schriener 2019].

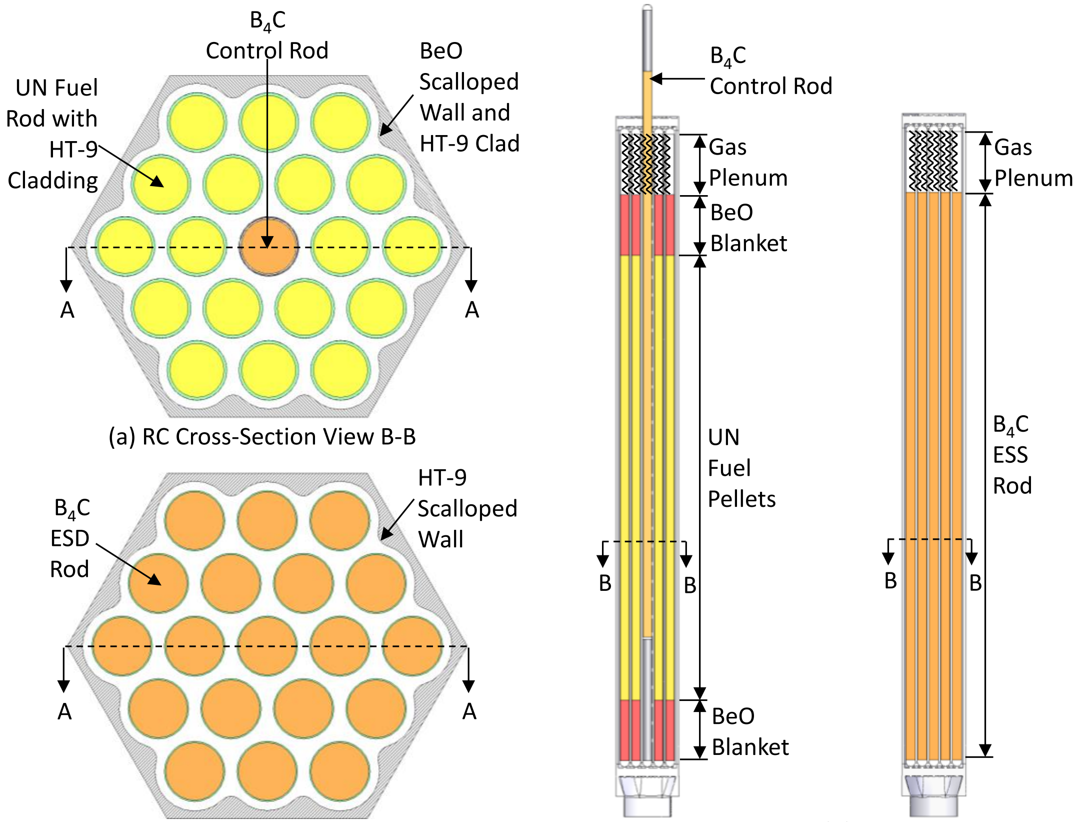

(a) RC Cross-Section View B-B

(b) ESD Cross-Section View B-B

(c) RC Cross-Section View A-A

(d) ESD Cross-Section View A-A

Fig. 3: Cross section and elevation views of the VSLLIM UN fuel assembly containing the B_4C reactor control rods and the center ESD assembly.

In addition, decay heat generated in the reactor core will be partially stored in the large mass of the in- vessel liquid sodium with several hundred degrees of temperature margin from the boiling point.

Furthermore, the alkali liquid metal heat pipes embedded in the primary vessel wall passively and redundantly transport a fraction of the reactor thermal energy during nominal operation and the decay heat after shutdown to a multitude of thermoelectric modules for generating auxiliary power. These modules, cooled by natural circulation of ambient air, can generate 10s of kW of auxiliary DC electric power, 24/7, for operating vital instruments and functions of the plant, independent of the onsite and off-site electrical power sources, and in the event of a toral station blackout [El-Genk and Palomino 2019; El-Genk, Schriener, and Palomino 2021].

The soft, fast neutron energy spectrum VSLLIM reactor core is loaded with 13.76 wt.% enriched UN fuel rods with HT-9 steel cladding arranged in a with P/D = 1.2 in hexagonal bundles with scalloped BeO walls (Fig. 3a). The walls help achieve a laterally uniform flow across the bundles [El-Genk and Palomino 2019]. The 54 full hexagonal bundles and the 6 partial bundles of UN fuel rods in the reactor core are arranged in 4 concentric rings. Each full bundle is loaded with 19 UN fuel rods and the partial bundles each are loaded with 12 rods (Fig. 3b). The reactor core fuel bundles are radially surrounded by BeO wedges within the HT-9 steel core barrel which serves as a radial neutron reflector (Fig. 3b).

The VSLLIM microreactor has two independent means for reactor control. The first is the 12 B_4C Reactor Control (RC) rods located in selected fuel bundles or assemblies within the second and third rings of the core (Fig. 2b, 3a and c). The HT-9 clad control rods replace the centermost UN fuel rod in these assemblies. The 12 B_4C control rods are divided into three groups identified as Groups A, B, and C and each has a separate drive motor (Fig. 2b). The control rods of naturally enriched B_4C pellets within HT-9 cladding have upper gas plenums to contain the helium generated by the neutron absorption in the Be during reactor operation. Group A is the three B_4C rods located in the second ring of fuel assemblies in the reactor core. Group B is the six B_4C rods in the third ring of the fuel assemblies adjacent to those of the Group A rods. Group C is the three B_4C rods in the fuel assemblies in the third ring of reactor core.

During reactor startup from cold clean condition, the Group B six control rods are partially withdrawn to bring the VSLLIM reactor core to criticality at zero power. Subsequently, the six control rods in Groups A and C are partially and gradually withdrawn simultaneously for the reactor core to increase the reactor thermal power to the desired nominal steady state value of 1.0 – 10 MW_{th}. The maximum withdrawal of these control rods is limited to 2/3 the core active height to speed reactor shutdown in case of an emergency, assisted with the inherent negative reactivity feedback in the reactor core.

For redundancy, the VSLLIM reactor core is provided with a central Emergency Shut Down (ESD) assembly of 19, HT-9 clad B_4C rods, 80% enriched in ^{10}B, with an HT-9 steel scalloped wall (Fig. 2, 3b and d). This assembly provides an independent means for shutting down the VSLLIM reactor in case of emergency. The ESD assembly is fully withdrawn from the reactor core prior to startup and is fully reinserted following nominal reactor shutdown. The next section details the developed dynamic model of the VSLLIM microreactor to generate training and testing data of the AI controller during a simulated startup transient of the VSLLIM reactor.

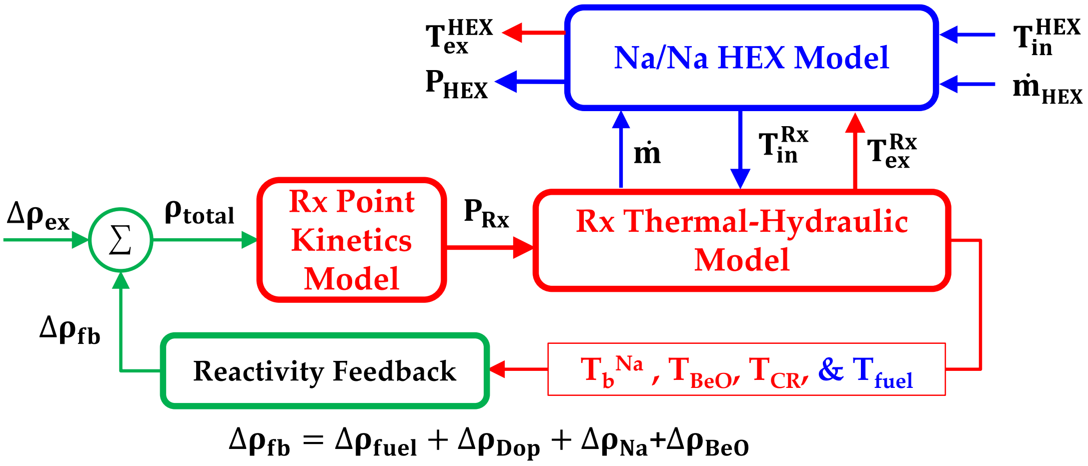

Fig. 4: A Block diagram of the various coupled sub-models of the developed VSLLIM transient model using MATLAB Simulink.

3. VSLLIM MATLAB Simulink Transient Model

The VSLLIM transient model couples 6-group point reactor kinetics and reactor thermal-hydraulics sub-models (Fig. 4). This model is developed using the versatile MATLAB Simulink platform [The MathWorks, 2022] for simultaneously solving the equations of these sub-models for the physics-based operation parameters of the reactor as functions of time during the simulated startup transients. These parameters are the reactor thermal power, the UN fuel and cladding average temperatures in the core, the mass flow rate and the inlet and exit temperatures of the in-vessel liquid sodium in the core, the chimney, the upper and lower plenums, and the downcomer. The reactor model also calculates the transient temperatures of the in-vessel Na/Na HEX solid structure and secondary liquid sodium flow and temperatures (Fig. 4). The VSLLIM transient Simulink model uses the ode23s modified Rosenbrock solver within Simulink with a timestep size of 0.02 s.

The solution of the reactor 6-group point-kinetics equations in VSLLIM transient Simulink model calculates the transient changes in the reactor fission power, P_{Rx}, in response to an active insertion of reactivity, $\Delta\rho_{ex}$, by partially withdrawing the group A and C control rods in the core and accounting for negative temperature reactivity feedback, $\Delta\rho_{fb}$, within the core (Fig. 4). The total reactivity, ρ_{total}, in the core equals the external reactivity minus the overall temperature reactivity feedback in the VSLLIM reactor core. The net temperature reactivity feedback is negative due to the decreases in the densities of the fuel, liquid sodium, and the Doppler broadening of the neutron cross sections in the UN fuel. Conversely, the temperature reactivity feedback of BeO in the radial and axial reflectors and walls of the

UN fuel assemblies is slightly positive and increases slowly with increased temperature [El-Genk and Palomino 2019].

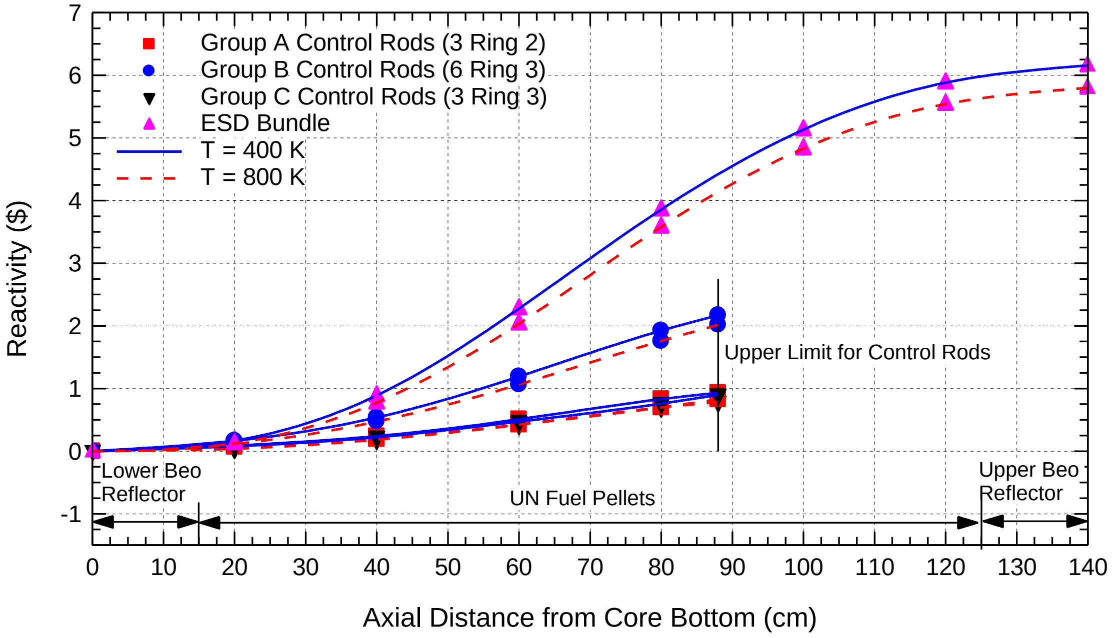

Fig. 5: Calculated reactivity worth of the VSLLIM control rod groups and the ESD assembly at mean isothermal temperatures of 400 and 800 K.

The reactivity worth of each of the control rod groups in the VSLLIM reactor core are determined as a function of the position and temperature using the MCNP6 code [Goorley 2014]. Fig. 5 plots the calculated reactivity worth for the Group A, B, and C control rods and the center ESD assembly as functions of the axial displacement and for temperatures of 400 and 800 K. The vertical lines indicate the upper limit of withdrawing the B_4C control rods in the core. The external reactivity insertion $\Delta\rho_{ex}$ is determined as a function of the displacement of the control rods and for the ESD bundle, assuming the control rods and HT-9 steel cladding and core structures are in thermal equilibrium at the mean temperature of the liquid sodium in the reactor core.

The point-kinetics sub-model solves the following equation for reactor fission power in terms of the fission yields, Y_i, and the decay constants, λ_i, of the six delayed neutron precursors, the prompt neutron lifetime, and as:

$$\frac{dP_{Rx}}{dt} = \left(\frac{\rho_{total} - \beta}{\Lambda}\right) P_{Rx} + \sum_{i=1}^{6} \lambda_i Y_i + S_0 \tag{1}$$

In this equation, S_0 is a fixed neutron source used for the reactor startup, β, is the total fraction of the of the delayed neutron precursors, given as $\left(\beta = \sum_{i=1}^{6} \beta_i\right)$, and Λ in the prompt neutron lifetime. The concentrations of the six delayed neutron precursors are obtained from the solution of the following six equations in terms of the reactor fission power:

$$\frac{dY_i}{dt} = \left(\frac{\beta_i}{\Lambda}\right) P_{Rx} - \lambda_i Y_i, \text{ where i=1 to 6} \tag{2}$$

The seven coupled reactor point-kinetics equations (Eq. 1 and 2) are solved for the reactor fission power, P_{Rx}, as a function of time during the startup and shutdown transients and following changes in external reactivity in the reactor core or the load power. The seven ordinary differential equations Eqs. 1 and 2 are solved using an efficient and robust approximation of the exponential matrix of 7th order-accurate Padé(3,3) approximate [El-Genk and Tournier 2016]. This approximate is not only accurate but also fast running and capable of handling large reactivity insertions with unrestrictive time step size. The kinetics parameters (Λ, β) in Eq. (1) and the spatial distributions of the fission power in the VSLLIM core are calculated by El-Genk and Palamino [2019] using the Monte-Carlo neutron transport code MCNP6 [Goorley 2014].

The VSLLIM reactor thermal-hydraulics sub-model accounts for the energy balance in the UN fuel rods, core structure, and the in-vessel sodium and for the momentum and mass balance of the circulating in-vessel liquid sodium in the reactor core. A 1-D sub-model for calculating the average UN fuel temperature in the core divides the average fuel rod into 11 axial nodes to account for the axial distribution of the fission power profile in the core and the increase in the temperature of the rising Na coolant in the core. The fission power generated in the UN fuel rods in the reactor core, P_{Rx}, is radially conducted to the pellet surface, and across the sodium radial gap and the HT-9 cladding and then convectively removed from the outer cladding surface by the circulating sodium in the reactor core. The transient changes in the mean temperature UN fuel in the average rod in the core, T_f, the radial sodium gap, T_{gap}, and the HT-9 cladding, T_c, are calculated from the solution of the following coupled 1st order differential equations, given as:

$$M_f C_{p,f} \frac{dT_f}{dt} = P_{Rx} - \frac{T_f - T_{gap}}{R_f + R_{gap}} \tag{3}$$

$$M_{gap} C_{p,gap} \frac{dT_{gap}}{dt} = \frac{T_f - T_{gap}}{R_f + R_{gap}} - \frac{T_{gap} - T_c}{R_{gap} + R_c} \tag{4}$$

$$M_c C_{p,c} \frac{dT_c}{dt} = \frac{T_{gap} - T_c}{R_{gap} + R_c} - P_c \tag{5}$$

In these equations R_f, R_{Na}, and R_c are the thermal resistance for the heat transfer in the UN fuel pellet, radial Na gap, and the HT-9 steel cladding, respectively. The rate of heat transfer at the outer surface of the cladding, P_C, equals that convectively removed by the circulating liquid sodium in the core, as:

$$P_c = h_c\, A_{c,o}\left[T_{c,o} - T_b\right] \tag{6}$$

The convective heat transfer coefficient, h_c, is determined using a recently reported correlation for alkali liquid metals in bundles of bare heated tubes [El-Genk and Schriener 2017], expressed as:

$$Nu = [10.7\ (P/D) - 7.1] + 0.024\left[1 - e^{-10.4((P/D)-1)}\right] Pe^{0.85} \tag{7}$$

This correlation is good agreement to within ±15% with more than 95% of 746 reported experimental data and the complied Nu values covering wide ranges of pitch-to-diameter ratio (P/D) (1.06 - 1.95) and Peclet number, Pe (4 – 3,074).

The overall energy balance equation for the in-vessel liquid sodium, assuming 5% loss of the fission reactor power due to the neutrons and gamma photons escaping the reactor, can be expressed as:

$$\mathrm{Q_{Rx}} = \mathrm{P_{Rx}}\,(0.95) = 2\,\dot{\mathrm{m}}\mathrm{C_p}(\mathrm{T_b} - \mathrm{T_{in}}) \tag{8}$$

In this expression, the reactor thermal power, $\mathrm{Q_{Rx}}$, equals 0.95 of the reactor fission power on the left-hand side, $\mathrm{P_{Rx}}$, calculated from the solution of the point- kinetic Eqs. 1 and 2. The driving pressure for natural circulation of the in-vessel liquid sodium driving pressure head, which the difference between the weights of the column of hotter, lower density sodium in the reactor core and chimney, and that of the colder, higher density sodium in the annular downcomer (Figs. 2a). These include the reactor core (Rx), the chimney (Ch), the upper and lower plenums, the Na/Na HEX and the downcomer (DC). Thus, the net driving pressure head for natural circulation of in-vessel liquid sodium is expressed as

$$\Delta\mathrm{p_d} = \left[\rho_{\mathrm{Na}}^{\mathrm{dc}}\mathrm{H_{dc}}\right]\mathrm{g} - \left[\rho_{\mathrm{Na}}^{\mathrm{Rx}}\mathrm{H_{Rx}} + \rho_{\mathrm{Na}}^{\mathrm{ch}}\mathrm{H_{ch}}\right]\mathrm{g} \tag{9}$$

The momentum balance of the circulating liquid sodium equates the driving pressure, $\Delta\mathrm{p_d}$, to the sum of the pressure losses, $\Delta\mathrm{p_{loss}}$, in the circulating in-vessel liquid sodium in different sections of the flow path. The expressions of the friction pressure losses in the VSLLIM transient model are given in Haskins and El-Genk [2017] and include the friction losses in the core, chimney, Na/Na HEX, the downcomer, and lower upper plenums (LP), as well as the pressure losses and gains due to flow area expansions and contractions along the flow path, $\sum\Delta\mathrm{p_{exp,con}}$. Thus, the momentum balance equation for VSLLIM can be expressed as:

$$\Delta\mathrm{p_d} = \Delta\mathrm{p_{loss}} = \Delta\mathrm{p_{loss}^{Rx}} + \Delta\mathrm{p_{loss}^{Ch}} + \Delta\mathrm{p_{loss}^{DC}} + \Delta\mathrm{p_{loss}^{LP}} + \sum\Delta\mathrm{p_{exp,con}} \tag{10}$$

The pressure loss terms on the right-hand side of this equation are expressed in terms of geometrical parameters, and the liquid sodium's kinematic viscosity and density at the local bulk temperatures in the various parts of the circulation path in the reactor. The solution of the coupled equations, 8, 9, and 10 calculations the circulation flow rate of the in-vessel liquid sodium, $\dot{\mathrm{m}}$, and temperatures in the different part of the circulation path (the reactor core, chimney, upper and lower plenums, the Na/Na HEX coiled tubes in the downcomer, the rest of the downcomer.

The Na/Na HEX model (Fig. 4) solves the energy balance equation for the Na flow inside the helical coils of the heat exchanger. It equates the heat transfer rate by convection from the circulating in-vessel Na on the shell side of the HEX coiled tubes to the rate of that the heat removed by flowing sodium inside the HEX tubes, $\mathrm{P_{HEX}}$, subject to the user specified inlet temperature, $\mathrm{T_{in}^{HEX}}$, and mass flow rate, $\dot{\mathrm{m}}_{\mathrm{HEX}}$, of the secondary sodium inside the tubes of the HEX. This model calculates the rate of heat removal from the in-vessel Na flowing through the HEX coils in the downcomer, P_{HEX}, and the temperature of the in-vessel liquid sodium exiting the HEX, T_{ex}^{HEX}, into the remainder of the downcomer then entering the reactor core through the lower plenum. The flow rate of the secondary liquid sodium inside the tubes of the Na/Na HEX is actively controlled for maintaining a constant reactor core inlet temperature, $T_{in} = 610$ K for the circulating in-vessel liquid sodium, and the user's specified inlet temperature and flow rate of the secondary Na inside the HEX coiled tubes.

3. VSLLIM Controllers

The VSLLIM reactor is controlled by two Programmable Logic Controllers (PLCs), namely: (1) the Na/Na HEX Na internal Flow and (2) PLC the Reactor Control PLC. The Na/Na HEX Flow PLC regulates the secondary Na flow rate inside the helical coils of the HEX by changing the current input to an electromagnetic or mechanical pump. A Proportional-Integral (PI) control function adjusts the inlet temperature and the flow rate of liquid Na inside the tunes of the HEX to maintain the temperature of the in-vessel liquid Na entering the reactor core constant at ~610 K during a reactor startup and nominal operation. The input to the PI controller is the difference between the in-vessel Na inlet temperature to the reactor core, T_{in}, and the temperature setpoint of 610 K.

The Reactor Control PLC regulates the displacements of the control rods in the reactor core and the ESD assembly to start up the reactor to the operator specified steady state thermal power level. It withdraws and inserts the ESD assembly and Group B control rods at constant rates of 4 mm/s and 2 mm/s, respectively. The PLC's logic changes the displacement of the Group A and C control rods to increase or decrease the reactor thermal power to the programed power setpoint, P_{SP}. When the reactor power, $P_{Rx} < 100$ kW$_{th}$ the controller withdraws Group A and C control rode from the reactor core at a constant rate of 2 mm/s. When $P_{Rx} \geq 100$ kW$_{th}$ the PLC uses a Proportional-Differential (PD) controller to manage the control rods displacement at a variable rate ≤ 0.5 mm/s, depending on the input to the PD of ($P_{SP} - P_{Rx}$). The PLC restricts the withdrawal of the control rods to help avoid a rapid increase in the total reactivity, ρ_{total}, into the core during a startup transient, using the criterion derived from a control scheme proposed by Bernard, Lanning, and Ray [1984] as:

$$\rho_{total} < \frac{1}{\alpha}\left[\frac{\left|\frac{d\rho}{dt}\right|}{\lambda_e} + \left|\frac{d\rho}{dt}\right| \tau \ln\frac{P_{SP}}{P_{Rx}}\right] \tag{11}$$

In this expression, α is a scaling coefficient, $\frac{d\rho}{dt}$ is the rate of change in reactivity, τ is the reactor period, and λ_e is the estimated effective decay constant for a delayed neutron group. The scaling coefficient, α, is adjusted to increase or decrease the total reactivity before the PLC halts the withdrawal of the control rods to provides time for the delayed negative temperature reactivity feedback in the

VSLLIM reactor by the thermal inertia of the system, to drop the total reactivity before further displacing the control rods.

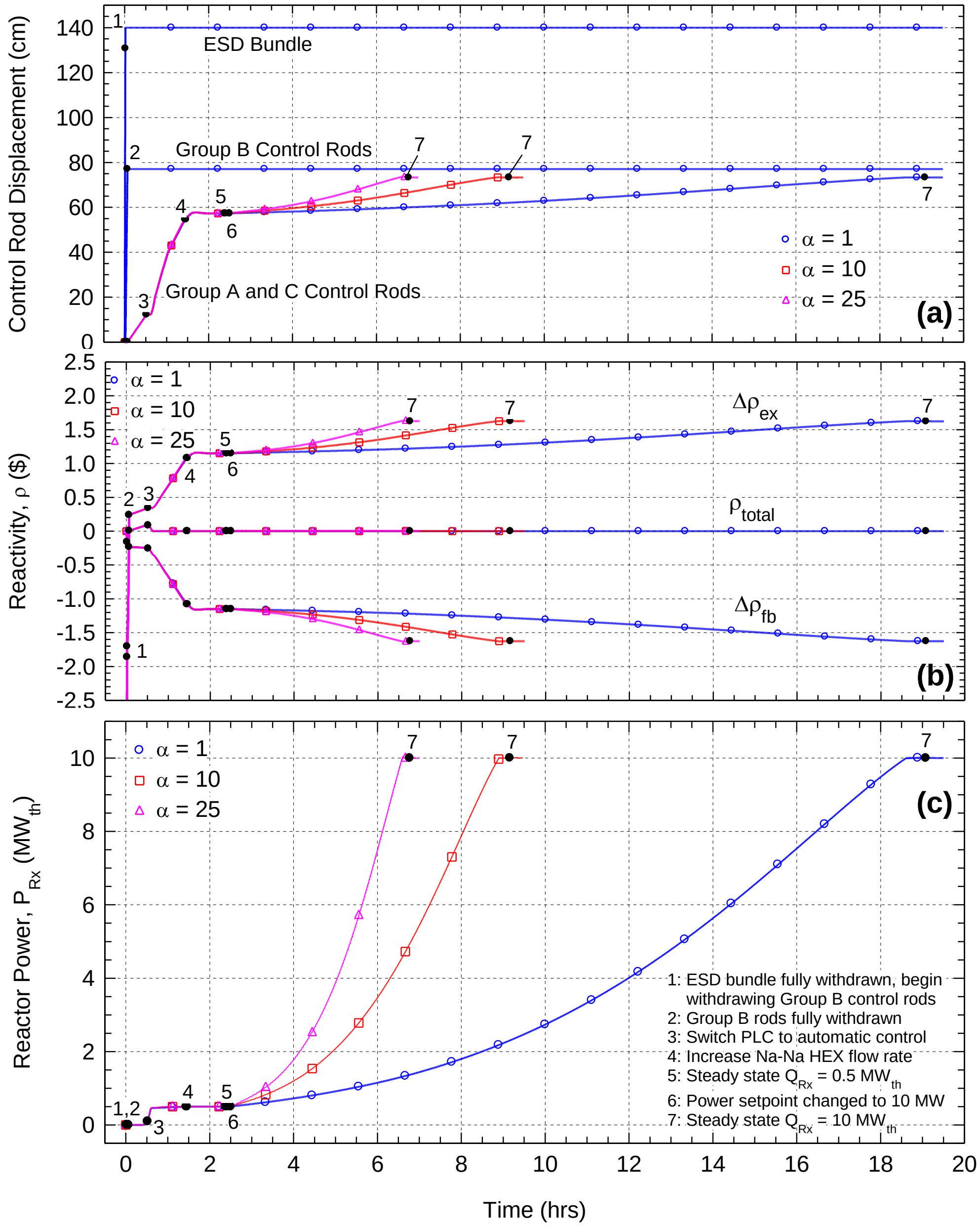

Fig. 6: Operation parameters of the control rod displacement, reactivity, and reactor thermal power in simulated startup transients of the VSLLIM reactor with different values of scaling coefficient, α, in the Reactor Control PLC.

4. VSLLIM Startup Procedure

A ML algorithm is used to train the artificial neural network to perform the functions of the Control PLC during a simulated startup of the VSLLIM reactor. The startup scenario for training the AI controller presents a challenging control application, considering the nonlinear nature of the reactor kinetics. The developed VSLLIM transient model in Simulink is used to simulate a reactor startup from initial subcritical condition to nominal steady state operation at a user specified reactor thermal power setpoint.

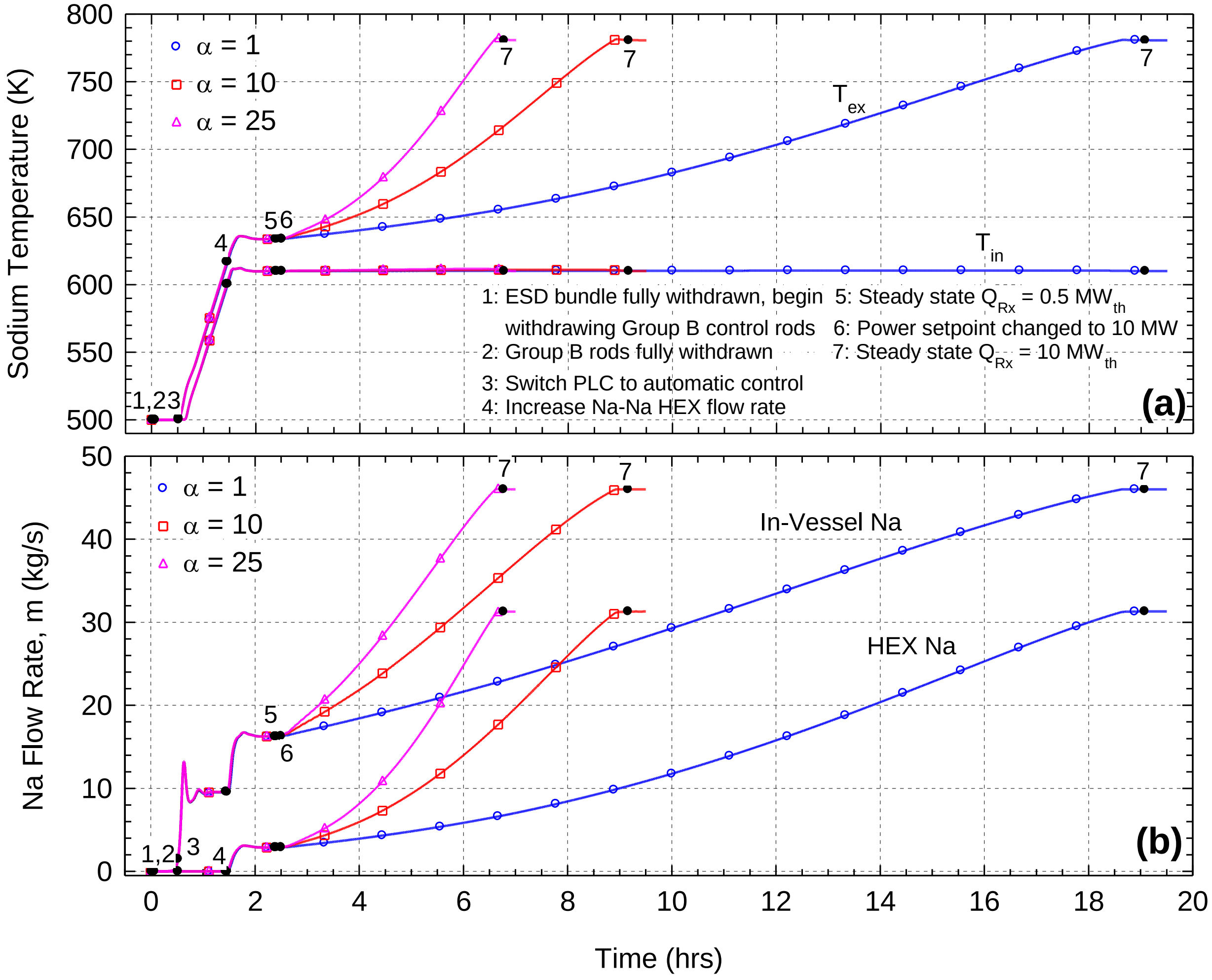

Fig. 7: Operation parameters of in-vessel sodium inlet and exit temperatures and mass flow rates in startup transients of the VSLLIM reactor with different values of scaling coefficient, α, in the Reactor Control PLC.

The reactor thermal power is increased first from critical condition at zero value to a low setpoint $P_{SP,1}$, and subsequently from the setpoint $P_{SP,1}$ to the desired steady state thermal power level $P_{SP,2}$. Bringing the reactor to steady state operation at the low power setpoint $P_{SP,1}$ provides time for the operators and the monitoring systems to ensure that the reactor power systems and the instrumentations on board are functioning properly before bringing the reactor to the desired power level $P_{SP,2}$.

The results in Figs. 6-7 are of the calculated changes in the operation parameters of the VSLLIM reactor in the simulated startup transients from with an initial power setpoint $P_{SP,1}$ = 0.5 MW_{th} to a final nominal steady state setpoint $P_{SP,2}$ = 10 MW_{th}. In the performed simulations, the scaling coefficient for the Reactor Control PLC, α, is set equal to 1, 10, and 25. Staring from zero flow in-vessel and HEX liquid sodium and 500 K uniform temperature, The Reactor Control PLC fully withdraws the ESD assembly from the reactor core at a constant speed of 20 mm/s (Point 1 in Figs. 6-7). At this point, the reactor is still subcritical, the Control PLC begins to partially withdraw Group B control rods from the reactor core at a constant rate of 4 mm/s until reaching criticality (Point 2 in Figs. 6-7). Next, the PLC Controller withdraws simultaneously Group A and C control rods at a constant rate of 2 mm/s until the reactor reaches nominal steady state power, P_{Rx} = 100 kW_{th} (Point 3 in Figs. 6-7). Subsequently, the control PLC switches to using the PD controller to regulate the displacement of the control rods in the core to bring the reactor thermal power to an initial $P_{SP,1}$ = 0.5 MW_{th}.

The present analyses investigated the effect of the value of the scaling coefficient α from 1 to 150 on the smoothness of the performance curves during the simulated startup transient and the time to reach the reactor thermal power setpoint. Fig. 8 shows the changes in the reactor thermal power Q_{Rx} during the simulated startup transients from an initial power setpoint $P_{SP,1}$ = 0.5 MW_{th} to a final power setpoint $P_{SP,2}$ = 10 MW_{th}. using the α = 1, 10, and 25. With α = 1, the controller brings the reactor thermal power up slowly and smoothly. With increasing α the controller increases the reactor thermal power faster but in a more 'scalloped' stair step fashion. This is the thermal inertia of the system delays the increase in the negative temperature reactivity feedback, ρ_{fb}, which slows the decrease in the total reactivity, ρ_{tot}, to prompt further withdrawal of the control rods (Eq. 12) (Fig. 8). With $\alpha > 50$ the reactor thermal power and temperatures not only increase less smooth during the simulated startup transients, but noticeably overshoot.

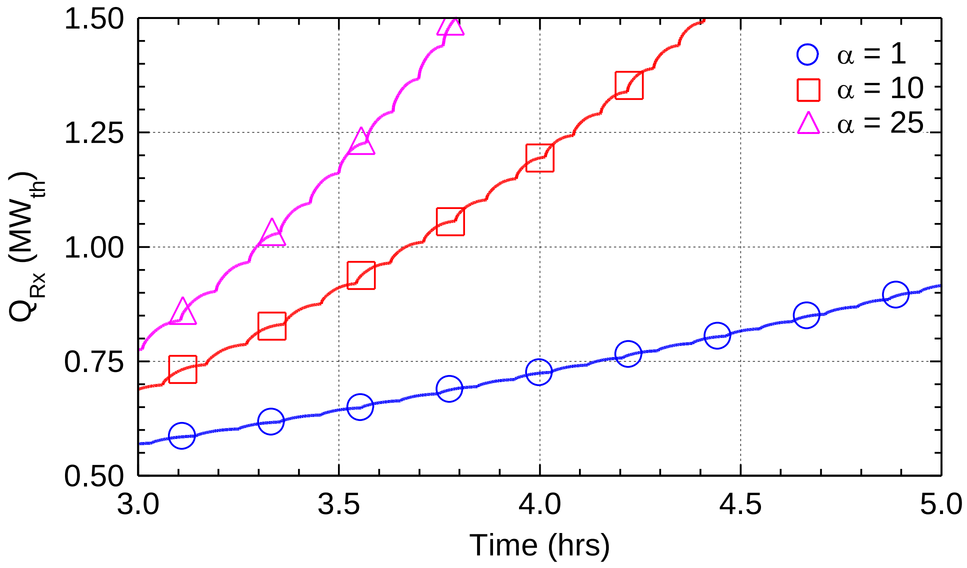

Fig. 8: Effect of the scaling coefficient α of the smoothness and the rise rate of the reactor thermal power during simulated startup transient of VSLLIM reactor.

On the other hand, increasing the value of α decreases the startup time to reach the nominal steady state reactor thermal power , Q_{Rx}, of 10 MW. Fig. 9 plots the startup time to reach nominal reactor steady state thermal power of 10 MW versus the value of α for the reactor PLC controller. The total startup time decreases rapidly from 19.0 hrs to 6.8 hrs as α increases from 1 to 25. Further increase in the value of α results in much smaller reductions in the startup time to 4.10 hrs with α = 100 and 4.02 hrs with α = 150. Therefore, a value of α = 25 is selected for the generation of the training data sets for the simulated startup transients of the VSLLIM reactor to different reactor thermal power setpoints ranging from 0.5 to 10 MW. This is because higher values of α slightly decrease the startup time and increase the reactor thermal power and temperatures to overshot as they approach their nominal steady state values.

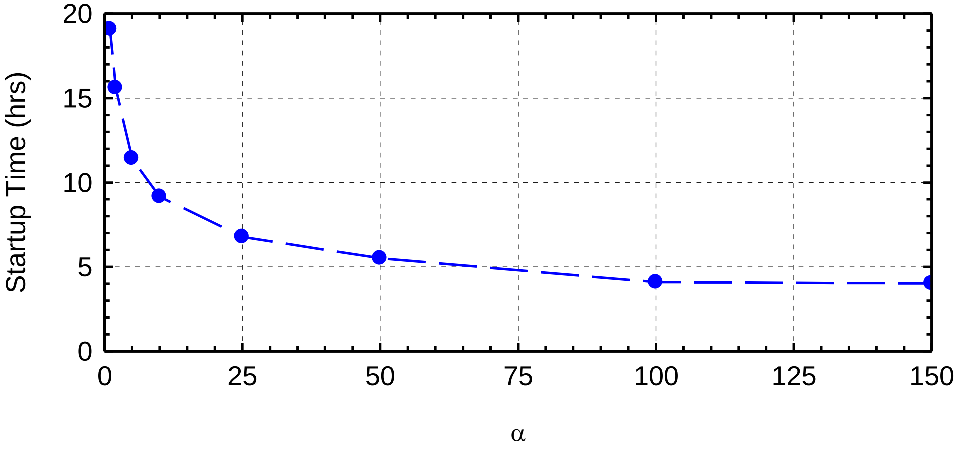

Fig. 9: Effect of the scaling coefficient values of the Reactor Control PLC, α, on the times of simulated startup transients of the VSLLIM reactor to reach a nominal steady state thermal power, Q_{Rx} of 10 MW.

5. Training Data of Machine Learning Algorithm

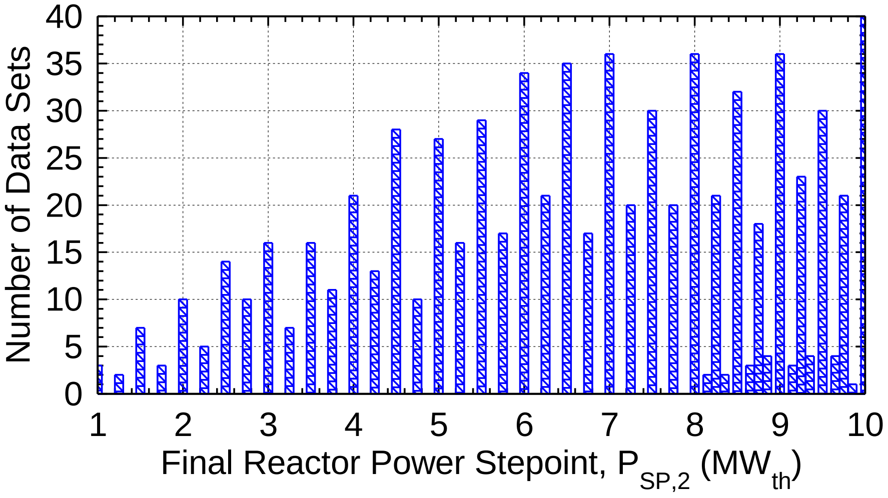

Fig. 10: Numbers of training data sets generated for different final reactor power setpoints, $P_{SP,2}$.

Developing a neural network-based AI controller for the VSLLIM reactor requires the generation of numerous data sets for the simulated reactor startup sequences to train the ML algorithm. The developed VSLLIM Simulink model generated many data sets with different reactor thermal power setpoint P_{SP} for training the ML algorithm. The training data sets are for a wide range of the low power setpoint $P_{SP,1}$ = 0.5 - 9.75 MW_{th}, and the higher power setpoint $P_{SP,2}$ = 1.0 - 10.0 MW_{th} in 0.25 MW_{th} increments. The generated data sets are also for different the reactor thermal power setpoints. A total of 797 startup transient data sets with more than 956 million data points. Fig. 10 shows the breakdown of the data sets generated for different reactor thermal power setpoint $P_{SP,2}$.

5.1 LSTM Algorithm

A ML algorithm is developed to train the AI neural network for PLC controller of the VSLLIM reactor for predicting the displacement of the control rods in the reactor core during simulated startup transients. The AI controller makes decisions on the displacement of the control rods based on the supplied real-time, sequential time data provided by the Simulink model. Recurrent Neural Networks (RNNs) are a class of ML algorithms used with sequential time-series data inputs [Amari 1972]. Long Short-Term Memory (LSTM) ML algorithms [Hochreiter and Schmidhuber 1997] are a category of the RNNs that have been investigated for control applications of nuclear power systems [Lee, Seong, Kim 2018; Radaideh, et al. 2020; Kim, et al. 2020; Zhang et al. 2020]. The algorithm passes the values for the hidden state and the cell state through the LSTM layers, with parameters determined when the cell state values are ‘remembered’ and ‘forgot’ to control the effect of long-term data dependencies on updating of the hidden state values. The ML program developed at UNM-ISNPS for the VSLLIM reactor implements the LSTM from the Pytorch 2.2 library [Paszke et al. 2017] into a python program for supervised learning and testing of the neural networks (Fig. 11).

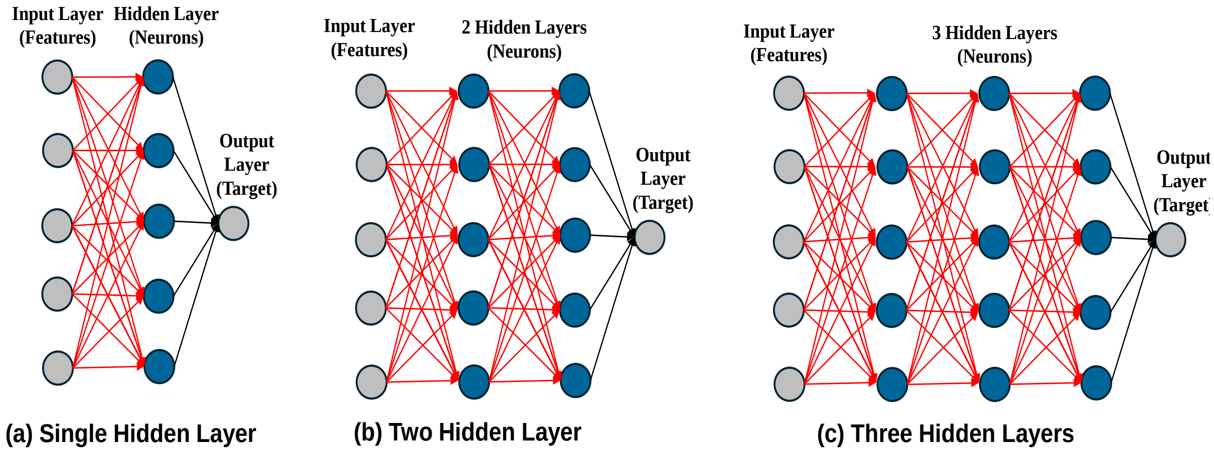

(a) Single Hidden Layer (b) Two Hidden Layer (c) Three Hidden Layers

Fig.11: Structure of the AI neural networks trained with five input features, 1, 2 or 3 hidden layers of neurons, and a single target output layer.

The implemented LSTM algorithm for ML is trained using the generated data sets by the VSLLIM Simulink model. Fig. 11 shows the connections for a layout of the neurons in the hidden layer of the neural network. The five input layer values to the neural network are referred to as the Features, and include the reactor power setpoint, the reactor thermal power, the circulation rate of the in-vessel liquid sodium in the reactor, and the reactor core sodium inlet and exit temperatures. The output layer is the displacement of the Group A and C control rods in the VSLLIM reactor core. The connections between the artificial neurons are defined by the determined values of the weight, w, and bias, b, coefficients for the neural network while training the network using the ML algorithm. In ML this is referred to as Supervised Learning where the network is trained using known values for Features and Target.

The data fed into the input layer is normalized relative to the output layer's highest and lowest values of each state variable for $P_{SP,1}$ = 0.5 MW_{th} and $P_{SP,2}$ = 10 MW_{th}. This same normalization is applied to all training data sets generated to ensure that the normalized data are consistently scaled. The implemented LSTM model used the Root Mean Square Error (RMSE) as the loss function and the AdamW optimizer with a weight decay constant = 0.1. The learning rate (LR) varied in the performed parametric analyses, which investigated both constant and variable LR values and implemented a scheduler which decreases the LR by an order of magnitude when the validation loss ceases to decrease for sequential epochs.

The time series data sets for the startup cases are divided into three groups, for Training, Validation, and Testing. During the Training, the weights and biases for the artificial neurons are updated based on the calculated RMSE or training loss of the predicted control rod displacement relative to the 'true' values in the VSLLIM Simulink generated datasets. During the Validation phase, the model calculates the RMSE or validation loss for the control rods displacement but does not update the weight and bias values. During each Epoch the ML algorithm cycles through all the Training and Validation data sets once. This process repeats for further epochs until the mean training and validation losses converge to a sufficiently low level. The performance of the trained neural network is analyzed in the Testing phase by determining the RMSE of the testing sets not included in either the training or validation data sets. This determines how well the neural network predicts the control rods displacement for cases it has not previously been exposed to. The implemented ML training approach divides the data sets into ~80% for training and ~20% randomly selected for validation, excluding the randomly selected sets placed aside for testing.

5.2 Parametric Analyses and Results

The optimization of an ML algorithm highly depends on a series of parameters. The performed analyses investigate the effect of different options on the weighted average accuracy of the algorithm and the accuracy of the VSLLIM controller (Table 1). Investigated are the effects of the Learning Rate (LR) of the ML algorithm, the length of lookback window sequence, the size of the training and validation data sets, using equal numbers of trainings sets for each final power setpoint $P_{SP,2}$, the order of the training sets loaded in to the ML algorithm, the number of neurons in the hidden layer and the number of hidden layers in the neural network, as well as including additional parameters as features. The effectiveness of the investigated options is evaluated both in terms of the weighted average accuracy of the testing results of the ML algorithm and the performance when they are integrated into a real-time AI controller coupled to the VSLLIM Simulink model. The testing phase independently calculates the accuracy of the control rod displacement determined by the trained AI model for each testing data set as well as the weighted average accuracies based either on the final power level or the initial power level during simulated startup. Table I summarizes the obtained results.

Table 1: Summary of the Parametric Analyses Results of the LSTM Machine Learning Algorithm and the Implementation into a Real-Time Controller for the VSLLIM transient model.

Parameter Investigated	Values	ML Training Results	Real-Time Controller Results
Learning Rate	• Constant LR = 0.001, and 0.1 • Variable LR Scheduler	• High initial learning rate results in validation loss not converging. • Implementing an LR scheduler decreased validation losses, training loss increased with increasing epochs. • With constant LR = 0.001 the training loss converged with time and validation loss is sufficiently low < ~ $1x10^{-4}$ to $1x10^{-3}$	N/A
Lookback Sequence Length Window	• 1, 5, 10, 20, 64, 250, 500	• The sequence window of ≤ 10 resulted in low testing accuracy. • Accuracy for sequence length of 64 is like that for 20, but training time increased. • With lookback windows of 250 and 500 points the ML algorithm failed during the data backpropagation step.	N/A
Number of Sets Used for Training	• Number of training sets from varied 10-626 and randomly selected and ordered	• Using a small number of training sets results in low testing accuracy • Increasing the number of testing sets from ~50 up to 626 slightly increases the spread in the accuracy values, with slight decrease in mean accuracy	N/A

Parameter Investigated	Values	ML Training Results	Real-Time Controller Results
Number of Training Sets for Different Power Levels	• 1,2,3,4,5 data sets for each of the 45 final power setpoints $P_{SP,2}$ • All models use same randomly selected set of 100 testing cases	• Weighted average accuracy increased and testing data accuracy spread decreased with increasing number of training sets per power, from 1 to 2. • Increasing number of trainings sets per power from 3 to 5 results in lower weighted average accuracy and increased spread in testing accuracy. • Highest weighted average accuracy is for 2-3 data points per setpoint final power	• ML models trained with 2 and 3 data sets per power level give comparable results. • Increasing number of data sets per power level up to 5 did not improve the rate of power increase during startup.
Order of Training Sets by Final Power Setpoint $P_{SP,2}$	• Low-to-high • High-to-low • Randomly shuffled	• Ordering the training data by $P_{SP,2}$ from low-to-high gives highest weighted average accuracy and lowest accuracy spread • Ordering data by $P_{SP,2}$ from high-to-low gives poor testing accuracy. • Random shuffling training sets resulted in accuracy values slightly below that of ordering low-to-high, but greater than for ordering high-to-low	N/A
Order of Training Sets by Initial Power Setpoint $P_{SP,1}$	• Low-to-high • High-to-low • Randomly shuffled.	• Ordering training data by $P_{SP,1}$ from low-to-high and high-to-low gives poor weighted average accuracy. • Random shuffling training cases with respect to $P_{SP,1}$ gives the highest testing accuracy and lowest spread.	N/A
Training on Sets for $P_{SP,2}$ = 10 MW_{th} Only	• Trained data on 35 random shuffled sets by $P_{SP,1}$	• High weighted average testing accuracy from > 99.7-99.8%. • Testing accuracy for cases with $P_{SP,2}$ < 10 MW is also high for data sets not included in the training or validation.	• With training on only the 10 MW data sets the controller gives a final P_{Rx} close to the 10 MW setpoint. • Testing for $P_{SP,2}$ < 10 MW the controller leveled at ~ 10 MW instead of the specified setpoint value

Parameter Investigated	Values	ML Training Results	Real-Time Controller Results
Neural Network Hidden Size	• 5, 10, 15, (h) 20, 25, 30 neurons in a single layer	• Increasing the number of neurons from 5 to 10 increases the weighted average accuracy and decreases the accuracy spread. • Using 10 neurons in the hidden layer gives the highest weighted average accuracy values. • Increasing the number of neurons from 10 to up to 30 shows a decreasing trend in the weighted average accuracy.	• The ML model with 10 neurons gives the highest weighted average accuracy, experiences large oscillations in the power and does not reach steady state operation. • Using 20 neurons in the hidden layer significantly improved the robustness of the controller's response, eliminated oscillations, with the controller leveling off at a constant power below the setpoint of 10 MW
Number of Hidden Layers in Neural Network	• (a) 2 Layers, 10 neurons/layer • (g) 2 Layers, 20 neurons/layer • (d) 3 Layers, 10 neurons/layer	• Increased number of hidden layers from 1 to 2 slightly increases the weighted average accuracy and decreases the spread in values. • Increasing the number of hidden layers from 2 to 3 gives similar weighted average accuracy as the 2-layer cases.	• Using 2 layers, 10 neurons/layer gives superior performance compared to 1 layer of 20 neurons, but the controller moves control rods at slower rate. • With 20 neurons/layer the controller both underestimates the final reactor power and experiences more power oscillations. • With 3 layers, 10 neurons/layer the controller withdraws control rods faster than with 2 layers, 10 neurons/layer.
Additional Input Parameters (Features)	• Derivatives of features, dP_{Rx}/dt, dT_{in}/dt, dT_{ex}/dt, $d\dot{m}/dt$ • ρ_{total} • (b) $\Delta\rho_{ex}$ • $\Delta\rho_{ex}$ and $\Delta\rho_{fb}$ • (f) Replace P_{SP} with $(Q_{Rx} - P_{SP})$	• Added features minor impact the weighted average accuracy for the testing cases	• With added derivatives of the primary features the controller shut down the reactor. • Including ρ_{total} as a feature also resulted in shutdown the reactor, • With $\Delta\rho_{ex}$ additional feature the controller performance improves,

Parameter Investigated	Values	ML Training Results	Real-Time Controller Results
	- (e) $\Delta\rho_{ex}$ and dP_{Rx}/dt - $\Delta\rho_{ex}$ and time		tracking closer to the desired ramp rate. - Adding both $\Delta\rho_{ex}$ and $\Delta\rho_{fb}$ as additional features caused the controller to oscillate the power. - Replacing the power setpoint P_{SP} with the difference between the reactor power and setpoint ($Q_{Rx} – P_{SP}$) slightly helped the controller to reach the correct final power but increased the mismatch of the increased power rate. - With both $\Delta\rho_{ex}$ and dP_{Rx}/dt additional features the controller increases the power at a remarkably high rate and overshoots the setpoint power. - With $\Delta\rho_{ex}$ and the simulation time added features the controller initially increases the power rapidly, then shut down the reactor to a subcritical state.

Figures 12 and 13 present selected examples of the testing results. The plots in Fig. 12 are for a training case with 1 hidden layer, 15 neurons/layer and a randomly selected group of 51 training cases, 9 validation data sets, and 100 testing sets. The presented results are for a learning rate of 0.001 and randomly shuffled training data sets. The red stars along the bottom axes of Figs. 12c and 12d show the number of testing cases for the values of $P_{SP,2}$ and $P_{SP,1}$. The training loss decreases to ~ $1x10^{-3}$ after 3 epochs with little change thereafter, the validation loss oscillates, and the predictions of the control rod displacement for one of the testing cases are in the good agreement of the values determined by the trained neural network.

Figs. 12c and 12d show the accuracy values plotted in increasing order for the final and initial power setpoints $P_{SP,2}$ and $P_{SP,1}$, respectively. The accuracy values show a spread between a minimum of 99.43%

and maximum of 99.93% for the 100 testing data sets cases. The average accuracy, weighted by the two power setpoints, are comparable, 99.82 and 99.86%.

Figure 13 compares the testing results for varying neurons structures and number of data sets per final power setpoint, $P_{SP,2}$ used for training. The cases with 2 data sets per setpoint power include 88 training sets, 10 validation sets, and 100 testing sets. The cases with 2 data sets per setpoint power includes 198 sets for training, 20 sets for validation and 100 training data sets. Changing the number of hidden layers of neurons from one to two (Fig. 9), for the case with 2 data sets per power level, increases the weighted average accuracy from 99.85% to 99.90% (Figs. 13a and b) and reduces the spread of the accuracy values, with the highest and lowest are 99.95% and 99.79%. Increasing the number of data sets per setpoint power in the training data sets slightly decreases the weighted average testing accuracy to 99.8% (Figs. 13c and d). It also increases the spread in the testing accuracy values for the same final or initial reactor power setpoint.

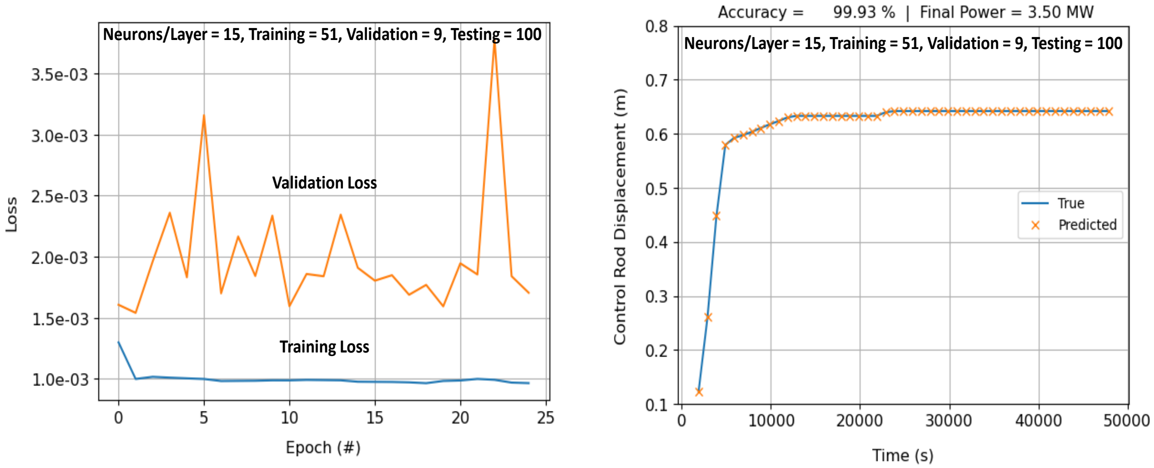

(a) Training Loss Convergence **(b) Predicted Control Rod Displacement**

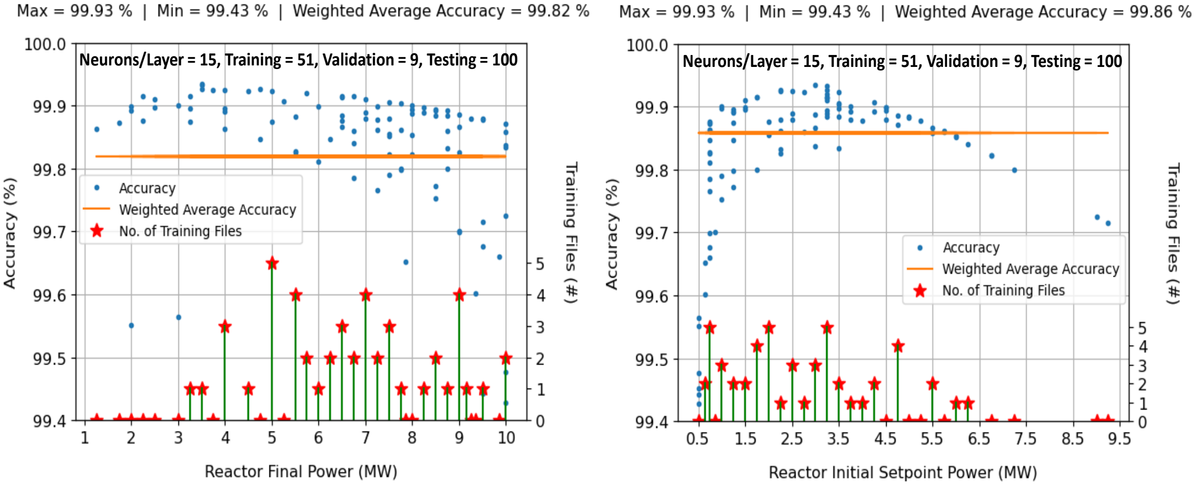

(c) Accuracy with Final Power $P_{SP,2}$ **(d) Accuracy with Initial Power Setpoint $P_{SP,1}$**

Fig. 12: ML training and testing results for 1 hidden layer, 15 neurons/layer, LR = 0.001 and randomly shuffled training data sets.

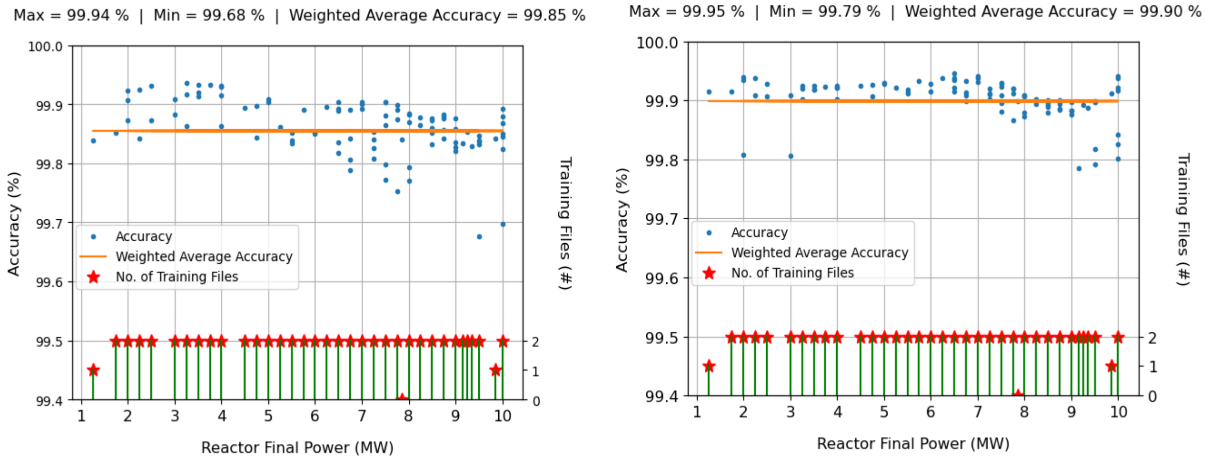

(a) 20 Neurons/layer, 1 Layer, 2 Training Sets/Power, Ordered Low-to-High

(b) 10 Neurons/layer, 2 Layers, 2 Training Sets/Power, Ordered Low-to-High

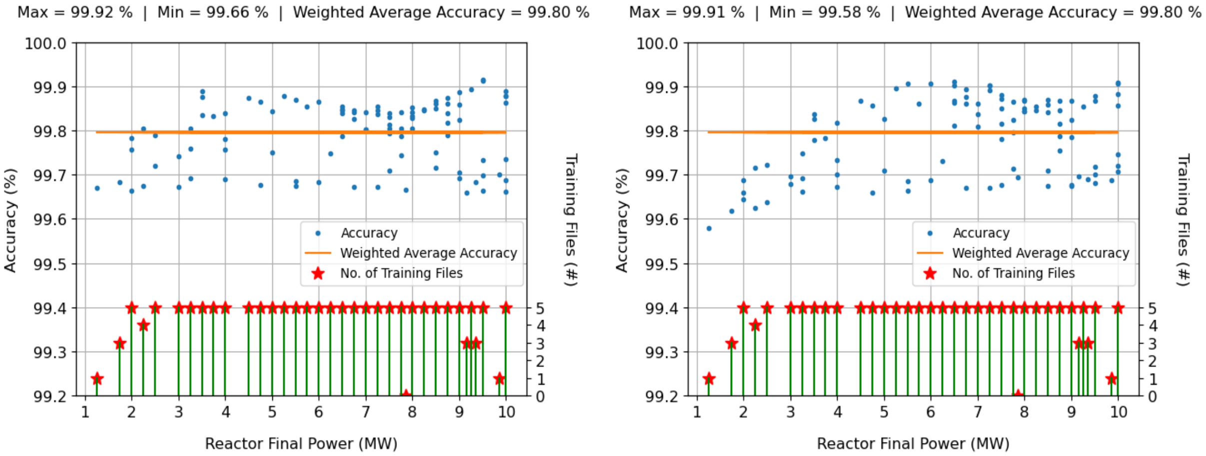

(c) 20 Neurons/layer, 1 Layer, 5 Training Sets/Power, Ordered Low-to-High

(d) 10 Neurons/layer, 2 Layers, 5 Training Sets/Power, Ordered Low-to-High

Fig. 13: Comparison of ML testing results for 1 layer, 20 neurons/layer and 2 layers, 10 neurons/layer, and 2 and 5 data sets per final power setpoint, $P_{SP,2}$.

5.2.1 Real-Time Testing of the Controller

Although the presented ML testing results show that the trained neural network can achieve a high weighted average accuracy of up to 99.9%, identifying which neural network will perform best requires evaluating their performance for real-time control of the VSLLIM Simulink model. The selected trained neural networks with high weighted average accuracies are integrated into a controller program coupled to the VSLLIM Simulink model. This is done using the LOBO Nuclear CyberSecurity (NCS) platform, developed by UNM-ISNPS in collaboration with Sandia National Laboratory [El-Genk and Schriener 2022a; Schriener and El-Genk 2022; El-Genk, Altamimi, and Schriener 2021; El-Genk and Schriener 2022b]. This platform's capabilities have been demonstrated for emulating autonomous control of a representative nuclear reactor power plant and investigating the response of the plant's digital control while under simulated cyberattacks. The LOBO NCS platform communicates between the computer running the controller program and the server running the real-time MATLAB Simulink model of the VSLLIM reactor. Such communication uses the Modbus Industrial Control System (ICS) communication protocol through an isolated Ethernet test network. The LOBO NCS platform synchronizes the timing of the VSLLIM MATLAB Simulink model to a real-time clock such that 20 ms simulation timestep takes 20 ms of physical wall time.

The trained neural networks using the data sets generated by the VSLLIM Simulink model for simulated startup transients are incorporated into a python controller program run on a fast Windows server. It communicates with the VSLLIM Simulink model running on an Ubuntu Linux server. The LOBO NCS platform receives the calculated operation parameters from the Simulink model at the end of each simulation timestep and writes them to the Modbus holding registers of the python controller program. In each repeated controller cycle, the program reads the simulation operation parameter values stored in Modbus holding registers and passes the generated data to the neural network to predict the control rods displacement. It also writes the control rods movement needed to the output Modbus holding registers to then be communicated back to the VSLLIM Simulink model to change the placement of the reactor control rods, commensurate with the external reactivity insertion in the reactor core.

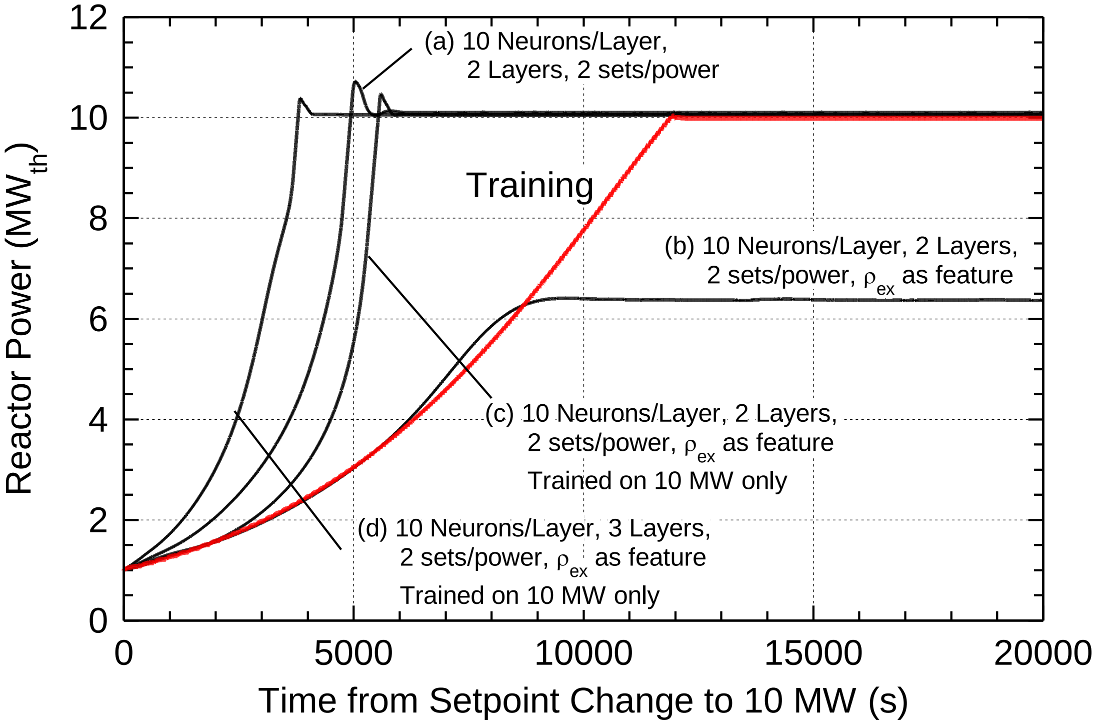

Fig. 14: Comparison of reactor power increase following setpoint change from 1 to 10 MW_{th} for trained real-time AI controller cases (a)-(d) in Table 1.

Testing results of the timing of the communication between the controller and the Simulink model determined that the controller's response to the transmitted values of the system parameters is commonly received by the Simulink model with a delay of 1-2, 20 ms timesteps. Thus, the controller can maintain a timely feedback response to the simulated startup transient given that the operation parameters do not change significantly during the delay period of 20 - 40 ms. The values received by the controller from the Simulink model during the last 20 timestep are set as lookback window sequence. In each controller cycle these values are passed to the neural network to determine the predicted rod displacement from the output layer of the neural network (Fig. 11).

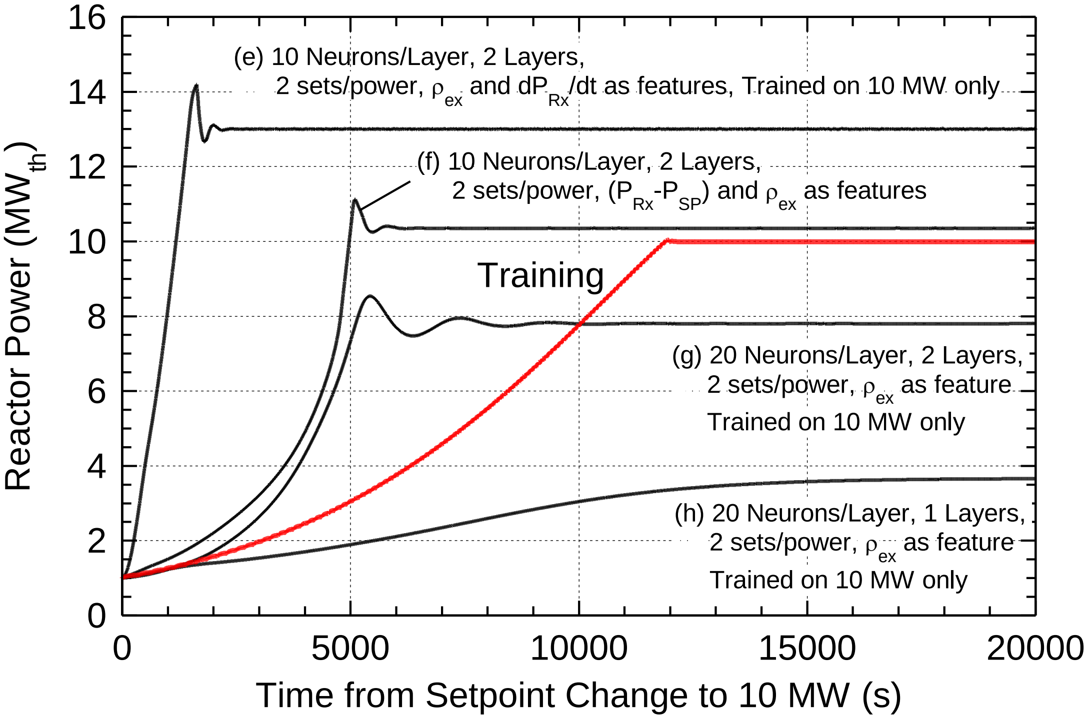

Fig. 15: Comparison of reactor power increase following setpoint change from 1 to 10 MW$_{th}$ for trained real-time AI controller cases (e)-(h) in Table 1.

Figures 14 and 15 compare the controller predictions of the VSLLIM thermal power of 8 of the 19 trained AI controller programs. Shown is the portion of the simulated startup scenarios where the AI controller attempts to increase the reactor thermal power to a steady state nominal values of 1 MW$_{th}$ up to 10 MW$_{th}$, commensurate with increasing the power setpoint P$_{SP}$ from 1 to 10 MW. The red curve in these figures is of the reactor thermal transient response during the simulated startup transient from 1.0 MW$_{th}$ to 10 MW$_{th}$ in the training data sets. The eight AI controller curves labeled (a)-(h) in Figures 14 and 15 correspond to the identified cases in Table 1.

In cases (a), (c), and (d) in Fig. 14 the trained controllers approximately achieve the correct final reactor power of 10 MW$_{th}$ but withdraw the Group A and C control rods at a more rapid rate, causing the reactor power to increase faster than the reference training data indicated by the red color curve in the Figure. Increasing the number of hidden layers of the ML algorithm (Fig. 11) from 2 (case c) to 3 (case d) causes the controllers to increase the reactor power more rapidly but at different rates, although the final steady state powers reached by AI controller are the same in the two cases.

Comparing cases (a) and (b) in Fig. 14 show that adding ρ_{ex} as additional feature causes the controller to track the correct reactor thermal power during the first 6,000 s following the change in the power setpoint, then the reactor power levels off at a low steady state value of only 6.37 MW_{th}, well below the setpoint of 10 MW_{th}. Case (e) in Fig. 15 includes the derivative of the reactor power and the external reactivity as additional features in the training date sets of the ML algorithm. The AI controller increases the reactor thermal power too quickly and overshoots the steady state reactor power to 13 MW_{th}. Changing the power setpoint to be the difference between the reactor power and the setpoint power (case f), decreases slightly the rate of increasing the reactor power compared to the actual rate and does not match the final power setpoint of 10 MW_{th}. The algorithms with 20 neurons/layer and 2 hidden layers (g) and 1 hidden layer (h) reach steady state reactor thermal power values below the setpoint power of 10 MW_{th}.

The obtained results so far show that supervised learning of the neural network using the LSTM algorithm show that the AI controller' response is highly sensitive to the training parameters. The obtained cases with minor differences in the ML testing accuracy give significant differences in the AI controller's responses, compared to the actual obtained using the VSLLIM transient model. Training the neural network therefore requires not only training ML algorithm using the generated transient data sets, but also reinforcing learning to improve the controller performance to match that generated by the developed VSLLIM model. This will be the focus of the present research in the next quarter.

6. Summary and Conclusions

This work developed, trained and evaluated an AI controller of the control rods displacement in the VSLLIM microreactor during simulated startup transients using a LSTM ML algorithm. The developed dynamic, physics-based model of the VSLLIM microreactor using the MATLAB Simulink platform simulates operation transients such as startup, shutdown, and changes in the reactor power level. In addition, the developed Programmable Logic Controllers for the VSLLIM transient model control the movement of the reactor control rods and ESD assembly in the reactor core and for adjusting the Na/Na HEX mass flow rate at a constant reactor inlet temperature of 610 K. To date the developed VSLLIM transient model and controllers are used to generate 797 startup transient data sets containing more than 956 million data values of the of the operation parameters of the reactors, .

The generated data sets are used to train the artificial neural network for the AI controller using an ML supervised training program using the LSTM model in the Pytorch 2.2 library. Parametric analyses investigated the effects of a wide range of training parameters, neuron structures, and training features the accuracy of the predicted control rods displacement and on the performance of the trained neural network integrated into an AI controller program. The AI controller coupled to the VSLLIM transient model using the LOBO NCS platform investigated the behavior of the trained neural network while receiving real-time feedback for displacing the reactor control rods.

The results for the trained neural networks integrated into the AI controller program show that achieving high ML testing accuracy with supervised learning from transient data sets does not necessarily result in a good real-time control performance for the trained neural network. Testing of the trained AI controllers with one layer of 10 neurons showed a weighted average accuracy of 99.9% but the AI controllers displaced the rods causing large oscillations of the reactor power. In the neural network structures, changing the arrangements and the number of neurons to either 1 layer of 20 neurons, 2 layers of 10 neurons/layer, or 3 payers of 10 neurons/layer eliminated the oscillatory behavior of the controller. The neural network structure with two layers and 10 neurons per layer provided the best performance in terms of the weighted average testing accuracy. Results also show that the proper choice of the features in the training data sets is essential realizing good real time controller performance, and that adding additional features in the training data sets can negatively impact the controller prediction and response.

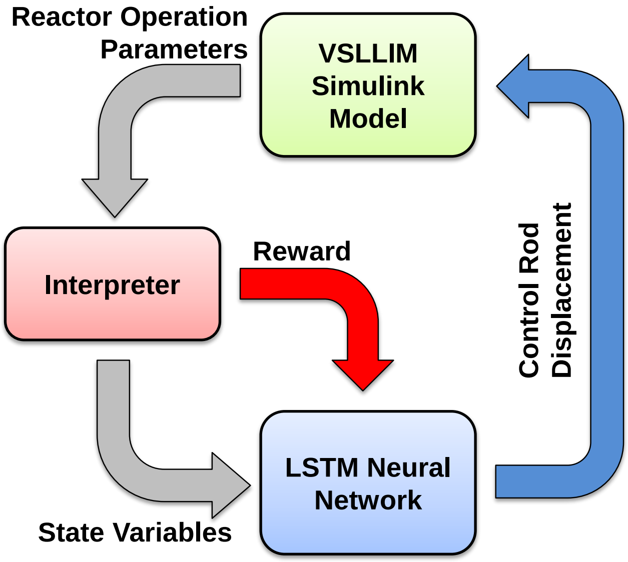

Fig. 16: Block diagram of the AI Controller with Reinforcement Learning function

While the trained neural networks can provide highly accurate static predictions, so far, the obtained research results demonstrate the limits of a supervised learning algorithm training using transient data to realize good real-time response of the reactor controller. Planned future effort will focus on enhancing the ML algorithm and controller to provide self-correcting behavior using a Reinforcement Learning function to adjust the weights and biases of the artificial neurons based on the feedback from the simulation model’s response. Fig. 16 shows a block diagram of the planned controller scheme with reinforcement learning function. The LSTM neural network will be based on a 2 layer, 10 neurons/layer structure, identified in the completed work so far to give the best performance The Supervised Learning ML algorithm will pre-train the neural network using the training data sets to determine the initial values of the weights and biases between the neurons as a function of time during simulated startup transients of the VSLLIM microreactor.

The reinforcement leaning structure of the controller (Fig. 16) will couple the connect the LSTM neural network to the VSLLIM transient Simulink model using the LOBO NCS platform. In each controller cycle, the calculated operation parameters by the VSLLIM transient model will be communicated to an Interpreter function to compare values of the state variables to the reference values in the training data sets (Fig. 16). The Interpreter provides feedback to the LSTM neural network using a reward function calculated based on the present and reference values of the operation parameters. In each controller cycle, reinforcement learning will adjust the neurons’ weights and biases to maximize this reward function. The adjusted neural network will then correct the displacement of the reactor control rods. The controller will be trained using the different startup transient of the VSLLIM reactor to help the reinforcement learning optimize the controller’ response. Future work will also investigate integrating the optimized AI controller into a remote-control system for a distant human operator to monitor and control the VSLLIM transient model and its autonomous control through a secure, encrypted connection.

References

Amari, S.-I., 1972, "Learning Patterns and Pattern Sequences by Self-Organizing Nets of Threshold Elements," IEEE Transactions on Computers, C(21), 1197–1206. doi:10.1109/T-C.1972.223477. S2CID 3708480.

Bernard, L.A., Lanning, D.D, Ray, A., 1984, “Digital Control of Power Transients in a Nuclear Reactor,” IEEE Transactions on Nuclear Science, NS-31(1), 701-705.

El-Genk, M.S., Altamimi, R., Schriener, T.M., 2021, “Pressurizer Dynamic Model and Emulated Programmable Logic Controllers for Nuclear Power Plants Cybersecurity Investigations,” Annals of Nuclear Energy, Vol. 154, 2021, 108121. https://doi.org/10.1016/j.anucene.2020.108121

El-Genk, M.S., Palomino, L.M., 2019, “A Walk-Away Safe, Very Small, Long-LIfe, Modular (VSLLIM) Reactor for Portable and Stationary Power,” Annals of Nuclear Energy, 129, pp. 181-198.

El-Genk, M.S. Schriener, T.M., 2017 "A Review of Experimental Data and Heat Transfer Correlations for Parallel Flow of Alkali Liquid Metals and Lead-Bismuth Eutectic in Bundles". J. Nuclear Engineering and Design, 317.

El-Genk, M.S., Schriener, T.M., 2022a, “A Cybersecurity Platform for Simulating Transient Responses of Emulated Programmable Logic Controllers in Instrumentation and Control Systems for a PWR Plant,” Journal of Cyber Security Technology, Vol. 6(1-2), 65-90. https://doi.org/10.1080/23742917.2022.2059323

El-Genk, M.S., Schriener, T.M., 2022b, “Modeling and Simulation Capabilities for Nuclear Cybersecurity Investigations of a Representative PWR Plant and Space Reactor Power Systems,” Nuclear Power Plants: Recent Progress and Future Directions, edited by J. K. Campton, Nova Science Publishers, Inc., Hauppauge, NY, USA, Ch. 1.

El-Genk, M.S., Schriener, T.M., Palomino, L.M., 2021. “Passive and Walk-Away Safe Small and Microreactors for Electricity Generation and Production of Process Heat for Industrial Uses.” J. of Nuclear Engineering and Radiation Science, 7(3), 031302.

El-Genk, M.S., Tournier, J.-M., "A Point Kinetics Model and Dynamic Simulation of Next Generation Nuclear Reactor". J. Progress in Nuclear Energy, 92, 91-103, 2016.

Goorley, T., 2014, “MCNP6.1.1-Beta Release Notes,” Technical Report LA-UR-14-24680. Los Alamos National Laboratory, Los Alamos, New Mexico, USA.

Haskins, D.A., El-Genk, M.S., 2017, "Natural Circulation Thermal-Hydraulics Model and Analyses of "SLIMM"- A Small Modular Reactor". Annals of Nuclear Energy, 101, 516-527.

Hochreiter, S., Schmidhuber, J., 1997, "Long Short-Term Memory". Neural Computation, 9(8): 1735–1780.

Kim, M., et al. 2020, “RNN-Based Online Anomaly Detection in Nuclear Reactors for Highly Imbalanced Datasets with Uncertainty,” Nuclear Engineering and Design, 364(1), 110699

Lee, D., Seong, P.H., Kim, J., 2018, “Autonomous Operation Algorithm for Safety Systems of Nuclear Power Plants by using Long-Short Term Memory and Function-Based Hierarchical Framework,” Annals of Nuclear Energy, 119. 287-299

Palomino, L., El-Genk, M.S., Schriener, T.M., 2019, “Post-Operation Dose Rate Estimates for the Very-small, Long-life, Modular (VSLLIM) Reactor,” ASME J. Nuclear Engineering and Radiation Science, NERS-19-1045

Paszke, Adam, et al. 2017, "Automatic Differentiation in Pytorch," In Proceedings of 31st Conference on Neural Information Processing Systems (NIPS 2017), Long Beach, CA, USA, Jan 24, 2018.

Radaideh, M.I, Pigg, C., Kozlowski, T., Deng, Y., Qu, A., 2020, “Neural-Based Time Series Forecasting of Loss of Coolant Accidents in Nuclear Power Plants,” Expert Systems with Applications, 160, 113699

Schriener, T.M., El-Genk, M.S., 2022, “Simulated False Data Injection Attacks on Emulated and Hardware Programmable Logic Controllers of the Pressurizer in a Representative Pressurized Water

Reactor Plant," Journal of Cyber Security Technology, 6(4), 216-241. https://doi.org/10.1080/23742917.2022.2123191

Zhang, J., et al., 2020, "Application of Cost-Sensitive LSTM in Water Level Prediction for Nuclear Reactor Pressurizer," Nuclear Engineering and Technology, 52(7), 1429-1435.